NeuroImage: Clinical 49 (2026) 103931

Contents lists available at ScienceDirect

NeuroImage: Clinical

journal homepage: www.elsevier.com/locate/ynicl

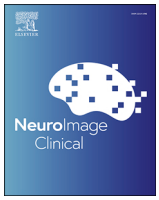

Simulating tDCS-induced electric fields in stroke patients: Realistic-lesion head models are needed

Ikko Kimura [a,1], Marcus Meinzer [b,1], Daria Antonenko [b], Robert Darkow [c], Agnes Flöel [b,d,2], Axel Thielscher [a,e,*,2]

[a] Danish Research Centre for Magnetic Resonance, Department of Radiology and Nuclear Medicine, Copenhagen University Hospital - Amager and Hvidovre, Copenhagen, Denmark
[b] Department of Neurology, University Medicine Greifswald, Greifswald, Germany
[c] FH Joanneum Gesellschaft mbH, Graz, Austria
[d] German Centre for Neurodegenerative Diseases (DZNE) Standort Greifswald, Greifswald, Germany
[e] Section for Magnetic Resonance, DTU Health Tech, Technical University of Denmark, Kgs Lyngby, Denmark

ARTICLE INFO

Keywords:
Aphasia
Transcranial electric stimulation
diffusion MRI
Neurorehabilitation
SimNIBS
Diffusion-to-conductivity mapping

ABSTRACT

Introduction: Transcranial direct current stimulation (tDCS) is tested as tool for post-stroke rehabilitation in aphasia, and individualized simulations of tDCS-induced electric fields (E-fields) can guide its application. However, the accuracy of simulations is challenged by complex and variable tissue properties of stroke lesions. Here, we assessed the impact of stroke lesions on tDCS-induced E-fields realistically in terms of lesion size, shape, and conductivity.

Methods: Structural and diffusion MRI datasets of stroke patients with aphasia (n = 13, six females, age = 38–70 years) and age-matched healthy controls (n = 13, eight females, age = 24–76 years) from a previous study were analyzed. Simulated E-fields were first compared between healthy head models with and without artificial lesions homogenously filled with cerebrospinal fluid. Then, the effects of lesion heterogeneity were tested by comparing E-fields for models of stroke patients with homogenous versus inhomogeneous (realistic) lesion conductivity informed by diffusion-to-conductivity mapping.

Results: Adding artificial lesions to healthy head models altered the E-field strengths (|E|) near the target region-of-interest (ROI) by up to 47%. Diffusion-to-conductivity mapping revealed substantial variability in lesion conductivities within and across patients. Modifying homogenous to realistic lesion models showed mostly small to moderate |E| differences within the ROI depending on montage type, lesion size, and lesion-to-target distance.

Conclusion: Stroke lesions affect tDCS-induced E-fields with substantial variability across montages and individuals. These findings support the use of head models that include realistic representations of the shape, size and conductivity of the lesions to improve the accuracy of individualized tDCS simulations and guide personalized stimulation protocols in stroke rehabilitation.

1. Introduction

Stroke is the most frequent cause of acquired impairment of language and communication (aphasia) and ~ 20–40 % of patients develop chronic symptoms, requiring long-term use of rehabilitation services (El Hachioui et al., 2013; Pedersen et al., 2004). Intensive and individually tailored speech-language therapy (SLT) can improve chronic aphasia (Brady et al., 2025, 2016), but recent clinical trials have also highlighted variable outcomes across patients and high percentages of non-responders (Breitenstein et al., 2017; Palmer et al., 2019; Rose et al., 2022). This has generated interest in adjunctive treatments capable of enhancing neuroplastic processes in aphasia, thereby rendering the lesioned brain more receptive to behavioral interventions (Crosson et al., 2019).

Based on studies in healthy individuals demonstrating that transcranial direct current stimulation (tDCS) can enhance language

* Corresponding author at: Ørsteds Plads, Building 345C, DK-2800 Kgs. Lyngby, Denmark.
E-mail address: axthi@dtu.dk (A. Thielscher).
[1] Equally contributed first authors.
[2] Equally contributed last authors.

https://doi.org/10.1016/j.nicl.2025.103931
Received 25 September 2025; Received in revised form 27 November 2025; Accepted 16 December 2025
Available online 23 December 2025

processing and learning (e.g., Flöel et al., 2008; Martin et al., 2017; Meinzer et al., 2014; Perceval et al., 2020, 2017), this approach has received substantial attention in aphasia research (Flöel et al., 2011; Meinzer et al., 2016; Brady et al., 2025; Elsner et al., 2019; Fridriksson et al., 2018). TDCS uses two or more scalp-attached electrodes to administer a weak electrical current to modulate excitability and neuroplasticity in target brain networks (Stagg and Nitsche, 2011). It is easy to administer and offers an effective placebo mode and an excellent safety profile, even in stroke patients (Antal et al., 2017). These features make tDCS an attractive tool for experimental or clinical studies in aphasia.

To date, dozens of aphasia trials that combined a wide variety of SLT and tDCS approaches have been completed (Meinzer et al., 2025). However, *meta*-analytic evidence for significant enhancement of SLT effects by tDCS is mixed and positive results have mainly been shown for specific linguistic functions like picture naming (Brady et al., 2025; Elsner et al., 2019; Raymer and Johnson, 2024), rather than functional communication abilities. Hence, a more personalized approach to using tDCS in post-stroke aphasia may be necessary.

For example, targeting of specific brain regions with tDCS can be aided by individualized computer simulations that estimate the distribution and intensity of the induced electrical field (E-field) using structural magnetic resonance imaging (MRI) data (Datta et al., 2011; Evans et al., 2023; Galletta et al., 2015; Krishnamurthy et al., 2025; Richardson et al., 2015; Minjoli et al., 2017). In treatment planning, these simulations can be valuable to ensure that the induced E-field is delivered to the intended target regions for tDCS and at a sufficient dose. However, the quality of E-field simulations critically depends on the validity of assumptions about the conductive properties of different tissue classes in the respective head models (Hunold et al., 2023). In stroke patients, this is further complicated by complex lesion shapes and sizes as well as variable tissue properties of the lesioned areas (Duering et al., 2020), that have not or only partly been accounted for in most previous studies (e.g., the lesion was classified as cerebrospinal fluid [CSF]; Evans et al., (2023); but see Krishnamurthy et al., (2021)).

In the present study, we used datasets of patients with post-stroke aphasia and age-matched healthy controls from a previous study (Darkow et al., 2017) to examine how stroke lesions influence tDCS-induced E-fields. Specifically, this study is comprised of two comparisons: (1) simulated E-fields from healthy head models with and without artificial homogeneous lesions derived from the stroke patients, and (2) those from head models of stroke patients with and without considering spatial heterogeneity of lesion conductivity. This study has three unique features. First, artificial lesions applied in this study are realistic in size and shape, in contrast to simplified lesion shapes applied in some of the previous studies (e.g., Evans et al., 2023). Second, we estimated the inter- and intra-individual variability of lesion conductivity using diffusion-to-conductivity mapping (Tuch et al., 2001). Third, we evaluated potential effects using focal montages (Niemann et al., 2024) as well as conventional bipolar montages. When aiming for personalized treatment planning, accurate patient-specific E-field calculations are required. Therefore, in addition to group-level differences, we also evaluated differences observed at the individual level.

2. Methods

2.1. Participants

We used an existing dataset of 16 S patients and a group of 16 age-matched healthy controls (Darkow et al., 2017). In this study, tDCS was administered over hand representation of the left primary motor cortex (M1) to assess the brain activity changes during a picture naming task. In this dataset, T1-weighted (T1w) and diffusion MRI (dMRI) data were obtained for chronic stroke patients and healthy controls. Three pairs of stroke patients and individually matched healthy controls were excluded because dMRI data were lacking in the patients (two pairs), or due to coregistration issues between dMRI and T1w data (one pair). This resulted in 13 pairs of stroke patients (six females; age: mean = 55.5 years, standard deviation [SD] = 10.0 years, 38–70 years; time since stroke: mean = 52.8 months, SD = 49.4 months, 12–169 months) and age-matched healthy controls (eight females; age: mean = 55.3 years, SD = 18.6 years, 24–76 years). A two-tailed paired *t*-test confirmed that there were no statistical differences in age between the 13 included stroke patients and the healthy controls (t_{12} = -0.02, P = 0.98).

2.2. Image acquisition

All T1w and dMRI data were collected using a Siemens Trio 3 T scanner equipped with a 16-channel array head coil (Siemens, Erlangen, Germany) in the Berlin Centre for Advanced Imaging of the Charité University Hospital. Detailed imaging protocols can be found in Darkow et al., (2017) for T1w. Briefly, T1w data were obtained with an MPRAGE sequence (voxel size = 1 × 1 × 1 mm^3, echo time [TE] = 2.52 msec, repetition time [TR] = 1900 msec, inversion time = 900 msec, flip angle = 9 degree). DMRI were recorded with a two-dimensional single-shot spin-echo echo-planar sequence (voxel size = 2.3 × 2.3 × 2.3 mm^3, matrix size = 96 × 96 × 61, b-value = 1000 s/mm^2, number of directions = 64, TR = 7500 ms, and TE = 86 ms).

2.3. Image preprocessing and generation of head models

T1w data were automatically segmented using *charm* implemented in SimNIBS (ver 4.1.0; Puonti et al., (2020)). This method segments the whole head into eight tissues (gray matter [GM], white matter [WM], CSF, compact bone, spongy bone, scalp, large blood vessels, eye muscles, and eye balls) to create a tetrahedral mesh representing the head anatomy (the "head model"). The CSF was further divided into ventricular and cortical CSF following Gregersen et al. (2024) to separate the ventricular CSF voxels from those that may contain meninges or were inside the lesion. The ventricular CSF was subsequently used to calibrate the diffusion-to-conductivity mappings in the stroke patients, as detailed in *2.5. Modeling of lesion conductivities using dMRI data*. For stroke patients, lesion masks from the previous study (Darkow et al., 2017), where the outlines of lesions were manually delineated by T1w and fluid attenuation inversion recovery (FLAIR) images, were added to the head model using the *add_tissues_to_upsampled* function in SimNIBS. These lesion masks were homogeneously filled with CSF (homogeneous-lesion head models).

DMRI data were preprocessed using *dwi2cond* from SimNIBS. This command mainly utilizes tools from the FMRIB Software Library (FSL; ver 6.0.4) (see Mosayebi-Samani et al., (2025) for details). In brief, dMRI data were eddy-current corrected, and co-registered to the T1w data. Here, distortion correction was not performed because images required for that process (non-diffusion weighted images with inverse phase encoding direction or field map) were not acquired in this dataset. Instead, dMRI data were non-linearly co-registered to the T1w data to mitigate the effect of B0 inhomogeneity-induced distortions using FNIRT with custom parameters.

2.4. Modification of healthy head models to assess effect of lesions on the E-field

To evaluate the effect of lesions on the E-field, artificial lesions were added to the head models of the healthy control group (i.e., healthy head models vs. homogeneous-lesion head models; Fig. 1A). To achieve realistic lesion shapes, the added lesion masks were created from the matched pair of stroke patients. Specifically, the lesion masks of the stroke patients were non-linearly transformed to the space of their matched healthy controls by first warping them to MNI space using *subject2mni* from SimNIBS, and then further to the matched healthy controls space using *mni2subject* in SimNIBS. Slight overlaps of the transformed lesion masks with the skull or scalp were excluded. The

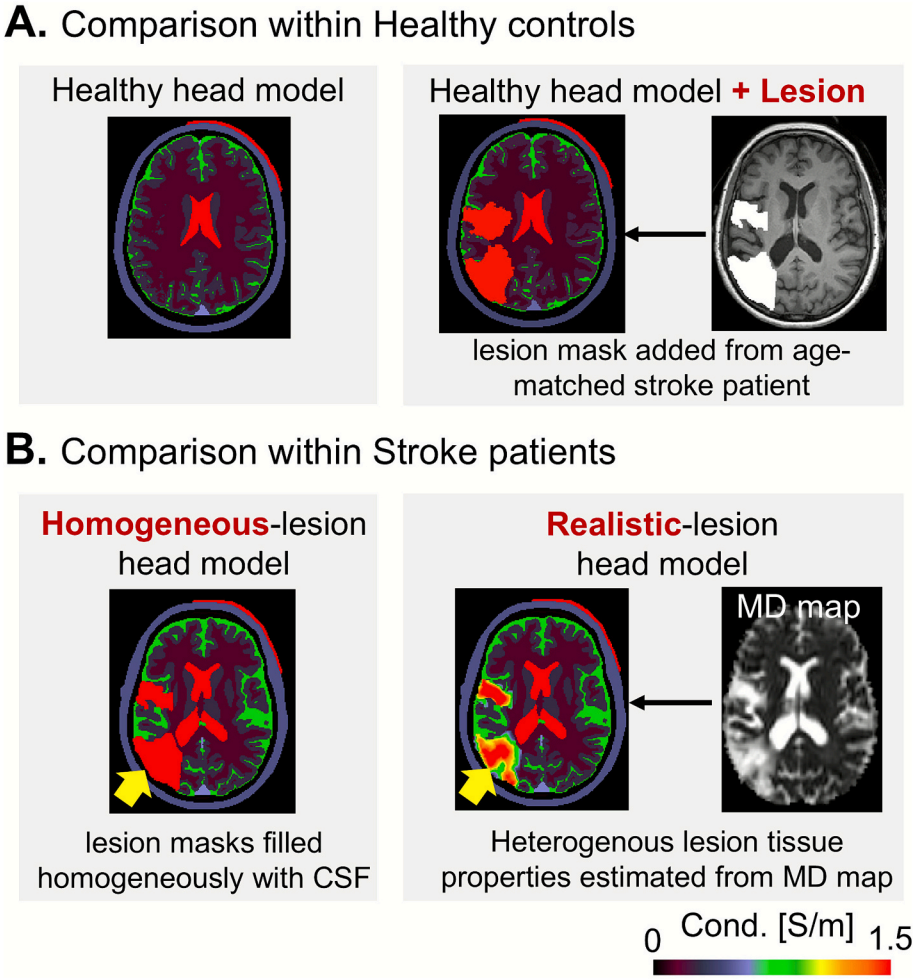

Fig. 1. Head models compared in this study. This study consists of two comparisons of simulated electric fields (E-fields): (A) Within head models of age-matched healthy controls of stroke patients, simulations were performed without (healthy head model) and with (healthy head model + lesion) artificially included lesions. To ensure realistic lesion shapes and sizes, we created the lesion masks by non-linearly transforming them from the age-matched stroke patients. (B) Within stroke patients, the simulated E-field was compared between head models with homogeneously (homogeneous-lesion head model) and realistically (realistic-lesion head model) modeled lesions (yellow arrows). The "homogeneous-lesion" head models set the conductivity of lesions to the conductivity of cerebrospinal fluid (CSF; left panel), while the "realistic-lesion" models estimated the conductivity within lesions from mean diffusivity (MD) maps derived from diffusion MRI. The figure in each panel represents the set conductivity for each head model. (For interpretation of the references to colour in this figure legend, the reader is referred to the web version of this article.)

final masks were added to the head models of the healthy controls using the same approach as for the homogeneous-lesion head models of the stroke patients (see *2.3. Image preprocessing and generation of head models* for details).

2.5. Modeling of lesion conductivities using dMRI data

The conductivity of lesions is usually modelled as homogeneous CSF. However, this is an over-simplification, as lesions usually consist of a mixture of CSF and various tissues, including scar tissue. To estimate the impact of this simplification on the simulated E-field, additional head models were created for the stroke patients. For these "realistic-lesion head models" (Fig. 1B), the spatially inhomogeneous and isotropic conductivities within the lesions were estimated from the dMRI data (diffusion-to-conductivity mapping). This was achieved by applying a linear relationship between the ohmic conductivity and the diffusivity of water, as measured by dMRI (Tuch et al., 2001):

$$\sigma_{ij} = b \bullet d_{ij} + c \quad (1)$$

Here, σ_{ij} and d_{ij} denote the j-th (j∈{1,2,3}) ohmic conductivity and diffusivity eigenvalues at voxel i, respectively. We assumed the conductivities within lesion masks to be isotropic, and hence estimated average conductivities across directions as follows:

$$\overline{\sigma_i} = b \bullet \overline{d_i} + c \quad (2)$$

$\overline{\sigma_i}$ and $\overline{d_i}$ represent the mean ohmic conductivity and the mean diffusivity (MD) at voxel i, respectively. As we presumed the conductivity of lesions to be between the conductivity of GM and CSF, the slope (b) and intercept (c) were estimated for each patient by fitting the literature values of conductivities of GM (0.275 S/m) and ventricular CSF (1.79 S/m) against their MD values (Supp. Fig. 8). We restricted CSF to the ventricles, because modeling studies suggested that thin cortical CSF area might be confounded with meninges (Jiang et al., 2020). Visual inspection of the fitted conductivities confirmed that they were in the expected range also for WM, which was left out from the fitting as control tissue (Supp. Fig. 8). The conductivity of cortical CSF was estimated to lie between that of GM and ventricular CSF. Finally, the conductivities within the lesions were estimated from the dMRI data using the fitted model, setting the upper and lower limit to be 1.79 S/m and 0.008 S/m (SimNIBS's default value for ventricular CSF and compact bone), respectively.

2.6. E-field simulations

Four electrode montages were used to simulate the E-fields induced by each tDCS montage, comprising two target locations [M1 or a personalized *peri*-lesional target derived from functional MRI], each with two types of montages [bipolar or focal montage] (Fig. 2A-D). Importantly, tDCS targeting M1 has been shown to modulate language processing in healthy individuals (Liuzzi et al., 2010; Meinzer et al., 2014) and to boost effects of speech and language rehabilitation in stroke patients with aphasia (Branscheidt et al., 2018; Hesse et al., 2007; Meinzer et al., 2016). The *peri*-lesional target was defined for each stroke patient as the location of the peak activation closest to the lesion, determined via functional MRI of a picture naming task in the previous study (Darkow et al., 2017; Fig. 2E).

This approach has widely been used in aphasia patients to target individually determined functional perilesional cortex (Baker et al., 2010; Fridriksson et al., 2018). The *peri*-lesional target locations were non-linearly transformed to the corresponding paired healthy controls. One participant was excluded for the montages of the *peri*-lesional target as there was no peak activated location near the lesions. Consequently, 12 pairs of stroke patients and their matched healthy controls were further analyzed for the analyses related to the *peri*-lesional target stimulation.

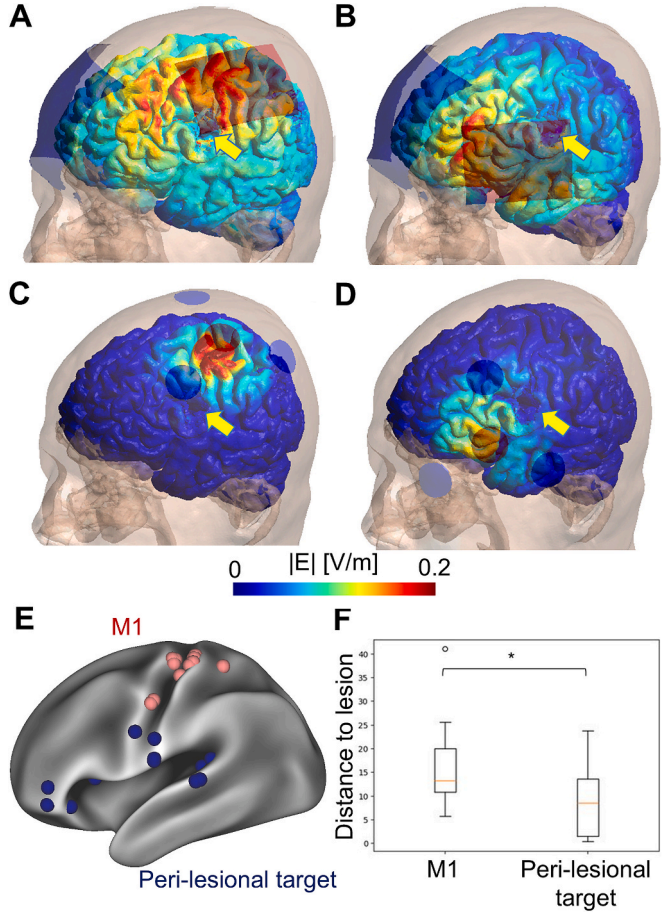

Fig. 2. Simulated montages. (A-D) represent the simulated electric fields (E-fields) on the gray matter in a representative stroke patient for the four tDCS montages applied in this study. We simulated the E-fields on bipolar montages targeting hand representation of the left primary motor cortex (M1; A) or the *peri*-lesional target (B), as well as focal montages placed above M1 (C) or the *peri*-lesional target (D). The red and blue electrodes indicate anodes and cathodes, respectively, and yellow arrows denote the lesion. (E) The M1 (red) and *peri*-lesional target locations (blue) for each stroke patient on the fsaverage_LR32k template. (F) Boxplot of the closest distance between the lesions and M1 or the *peri*-lesional targets. * $P < 0.05$. (For interpretation of the references to colour in this figure legend, the reader is referred to the web version of this article.)

For the bipolar montages, the anode was located over the target location, while the cathode was placed on the right supraorbital area (just above the right eyebrow) using rectangular rubber electrodes (anode: 5 × 7 cm^2, cathode: 10 × 8 cm^2; Fig. 2A and B). For the focal montages, the anode was positioned over the target location, while the three cathodes were equally distributed with a radius 4.5 cm using the SimNIBS function *tDCS_Nx1.py* (Niemann et al., 2024; Fig. 2C and D). One of the cathodes in the focal montage was placed in the direction of C3 to C1 for M1, while it was in the direction of left pre-auricular to T7 for the *peri*-lesional target. All rubber electrodes used in the focal montage were assumed to be circular with a radius of 12.5 mm. For M1 stimulation, the anode was located at C3 for the bipolar montages following Darkow et al. (2017), while it was placed over the left hand-knob for the focal montages (Niemann et al., 2024). For *peri*-lesional target stimulation, the anode was centered over the individual *peri*-lesional target for both the bipolar and focal montages.

The finite element method implemented in SimNIBS was used to simulate the E-field induced by each montage of tDCS (Thielscher et al., 2015). All rubber electrodes were assumed to be two mm thick with one mm of electrode gel. The default conductivity values in SimNIBS were applied for the simulation, unless otherwise noted. The conductivity was set to 0.85 S/m for cortical CSF (Jiang et al., 2020) and 1.79 S/m for ventricular CSF (Baumann et al., 1997), and was modeled isotropically for both GM and WM using their standard values in SimNIBS. In the homogeneous-lesion head model for the healthy controls and stroke patients, the lesion conductivity was fixed to 1.79 S/m, which corresponds to the conductivity of ventricular CSF as described above. For the bipolar montages, the stimulation currents injected into the electrodes were set to ± 1 mA. For the focal montages, the current injected into the anode was set to 1 mA and that of each cathode to −1/3 mA. The magnitude (|E|) and normal component (nE) of the E-field (Antonenko et al., 2019) were extracted at the middle layer of the cerebral cortices (i.e., the midpoint of pial and white surfaces; cortical middle layer) of both hemispheres for further analyses. For healthy controls, the cortical surface areas corresponding to the artificially added lesions were excluded.

Differences in the simulated E-fields were assessed between (1) head models of healthy controls with versus without artificially added lesions (Fig. 1A), or (2) head models of patients with homogenously versus realistically modelled lesions (Fig. 1B). For both cases, E-fields were simulated for the bipolar and focal montages and compared. For analysis, global (across overall grey matter) and local (nearby the target location) metrics of the E-field differences at the cortical middle layer were extracted. For the global metrics, the peak value and focality of |E| within the cerebral cortex were calculated. Using SimNIBS's default settings, the peak value was defined as the 95th percentile of |E|, while the focality was defined as the area where |E| exceeds 75 % of the 95th percentile of |E|. For the local metrics, |E| or nE at the cortical middle layer was extracted within region-of-interests (ROIs). The ROIs were defined for each montage as a 12.5 mm radius sphere centered at the target location (M1 or the *peri*-lesional target), with the size matched to the size of the electrodes in the focal montages (Niemann et al., 2024). Two measures were used for assessing the E-field differences between the head models within a ROI:

First, the *difference of the average E-field strength in the ROI* was calculated:

$$\Delta\text{mean}\,|E| = \frac{\sum_{i\in ROI}|E(i,headmodel1)|}{\#voxelsinROI} - \frac{\sum_{i\in ROI}|E(i,headmodel2)|)}{\#voxelsinROI} \quad (3)$$

Here, head models 1 and 2 are the healthy head model with and without artificial lesions, respectively, or the patient head model with realistic and homogeneous lesions, respectively. In addition to changes of the

average E-field strength, changes of the average normal component within the ROI (denoted as Δ mean nE) were calculated in the same way.

Second, the E-field differences were determined at each location in the ROI, and the average of their absolute values was calculated:

$$\text{mean}\,|\Delta|\mathrm{E}|| = \frac{\sum_{i\in ROI}||\mathrm{E}(i,headmodel1)| - |\mathrm{E}(i,headmodel2)||}{\#voxelsinROI} \quad (4)$$

In contrast to eq. (3), this *average of the location-wise E-field differences in the ROI* is sensitive also to changes of the E-field pattern within the ROI. For example, if the lesion increased the E-field in some locations and decreased it in others within the ROI, these differences can cancel each other out in Δ mean |E|, but not in mean |Δ| E||. Changes of the average of the location-wise differences of the normal component (denoted as mean |Δ nE|) were calculated in the same way as stated in eq. (4).

For both measures, the relative differences compared to the healthy head model or the homogeneous-lesion head model (Evans et al., 2023) were calculated to relate the size of the lesion-related differences to the baseline E-fields. These measures enable us to more easily relate our simulation results that used a fixed current of 1 mA to the varying intensities applied in practice. We defined relative differences of 10–25 % and > 25 % in |E| or nE as *moderate* and *large*, respectively. This approach was motivated by previous literature suggesting that E-field differences of 25 % can lead to relevant differences in the physiological and behavioral tDCS effects (Antonenko et al., 2019; Caulfield et al., 2022; Laakso et al., 2019). For example, a significant difference in tDCS effects on working memory was demonstrated between high and low E-field groups (|E| in high E-field group: mean = 0.25 V/m, range = 0.22–0.31 V/m; |E| in low E-field group: mean = 0.18 V/m, range = 0.16–0.22; Caulfield et al., 2022). Thus, we term field differences exceeding 25 % as *large* to indicate that E-field simulations need to be accurate to at least this level to ensure reliable dose quantification and optimization. Correspondingly, we term E-field changes within the 10–25 % range as *moderate*, as simulation errors in that range can still noticeably affect the analyses of dose–response relationships. Of note, we use the terms *large* and *moderate* to roughly relate the observed impact of different lesion models on the E-fields to the required level of simulation accuracy. They do not indicate assumed physiological or clinical effectiveness.

2.7. Statistical analysis

Two-tailed one-sample t-tests were used to detect consistent increases or decreases in the global and local difference measures across participants. Two-tailed two-sample t-tests were applied to evaluate whether the measures or differences in the measures were different across bipolar and focal montages for each target location (M1 or *peri*-lesional target). As the local difference metrics showed high inter-individual variability in both stroke patients and healthy controls (see Results), Spearman's correlation coefficients were additionally calculated between the inter-individual variations in the difference in local metrics within the ROI and anatomical lesion features. The following lesion features were used: (1) lesion size in mm3, (2) lesion-to-target distance in mm (i.e., the shortest distance between a target and lesion masks), and (3) mean absolute conductivity difference within lesion masks in S/m. As these are exploratory analyses, $P < 0.05$ uncorrected for multiple comparisons was set as threshold for statistical significance. Statistical functions in SciPy (ver 1.10.1) and JASP (ver. 0.18.3 for Windows) were used for all statistical analysis.

3. Results

3.1. Differences in E-fields between head models with and without lesions

Compared to the stroke patients, the artificially created lesions in the age-matched healthy controls were not significantly different in the size (t_{12} = -0.52, $P = 0.61$; Supp. Fig. 5A) or the distances to M1 (t_{12} = -1.15, $P = 0.27$; Supp. Fig. 5B) or the *peri*-lesional target (t_{11} = -1.15, $P = 0.15$; Supp. Fig. 5C). This suggests that the main lesion features were maintained even after transforming the lesions from the stroke patients to the age-matched healthy controls. Between the head models with and without artificial lesions, the mean absolute difference in conductivity within the region of the artificial lesions showed small variability across the participants (mean = 1.55 S/m, SD = 0.05 S/m, 1.48–1.63 S/m).

Global metrics: Adding the lesions to the healthy head models changed the 95 % peak |E| by up to 15 %, 27 %, 34 %, and 31 % for the bipolar M1, focal M1, bipolar *peri*-lesional target, and focal *peri*-lesional target montages, respectively (Supp. Fig. 6C). In most participants, adding lesions reduced the 95 % peak |E| (bipolar M1: t_{12} = -3.18, $P = 0.008$; focal M1: t_{12} = -3.87, $P = 0.002$; bipolar *peri*-lesional target: t_{11} = -3.09, $P = 0.010$; focal *peri*-lesional target: t_{11} = -5.08, $P < 0.001$; Supp. Fig. 6B). Adding lesions also changed the 75 % focality of |E| by a maximum of 50 %, 9.0 %, 30 %, and 18 % for the bipolar M1, focal M1, bipolar *peri*-lesional target, and focal *peri*-lesional target, respectively (Supp. Fig. 7C). The focality metrics were both increased and decreased by adding lesions depending on participants (Supp. Fig. 7B).

Effects on the average E-field in the ROIs (Δmean |E|; eq. (3): Fig. 3A shows the average E-field strengths in the ROIs for the healthy head models with and without artificial lesions in montages targeting M1. Across participants, tDCS induced an average E-field strength of ~ 0.2 V/m in the ROIs (bipolar: mean = 0.22 V/m, SD = 0.04 V/m; focal: mean = 0.20 V/m, SD = 0.08 V/m). Adding lesions led to both decreases and increases of the average E-field in the ROIs (Table 1) depending on the relative location of lesions (Fig. 4), which is in line with Evans et al. (2023). More specifically, adding lesions consistently decreased the average E-field strength in the ROIs across participants in the bipolar montage, while it was not consistently increased or decreased in the focal one. The differences corresponded to relative changes by maximally 31 % and 17 % for the bipolar and focal montages, respectively. The findings for nE were qualitatively similar to those reported here for |E| and are therefore reported in the Supplementary information.

Fig. 3C shows the average E-field strength in the ROIs for the healthy head models with and without artificial lesions in montages targeting the *peri*-lesional target. As for the montages targeting M1, tDCS induced an average E-field strength of ~ 0.2 V/m in the ROIs (bipolar: mean = 0.20 V/m, SD = 0.04 V/m; focal: mean = 0.19 V/m, SD = 0.07 V/m). Artificial lesions also induced both decreases and increases of the average E-field strength (Table 1). The differences corresponded to relative changes of maximally 43 % and 47 % for the bipolar and focal montages, respectively.

We then explored associations between the differences in the average E-field strengths in the ROIs and the anatomical lesion features (Supp. Table 1). The absolute change in the average E-field strengths due to the added lesions was significantly correlated to the lesion-to-target distance for both the bipolar and focal M1 montages. The other correlations were not significant.

Average of the location-wise E-field differences in the ROIs (mean |Δ|E||; eq. 4): In montages targeting M1, the average of the location-wise E-field strength difference was significantly higher in the bipolar montage than the focal one (Table 2). Stated in percent of the baseline E-field without lesions, the differences were up to 32 % and 21 % for the bipolar and focal montages, respectively (Fig. 3B; Table 2). Regarding montages targeting the *peri*-lesional target, the differences were similar for the bipolar and focal montages and reached up to 44 % and 47 %, respectively (Fig. 3D; Table 2).

Spearman's correlation coefficients (Table 3) demonstrated that the differences were significantly positively correlated to the lesion size in three out of four montages. They were also significantly negatively correlated with the lesion-to-target distance in three montages. The remaining correlations were not significant.

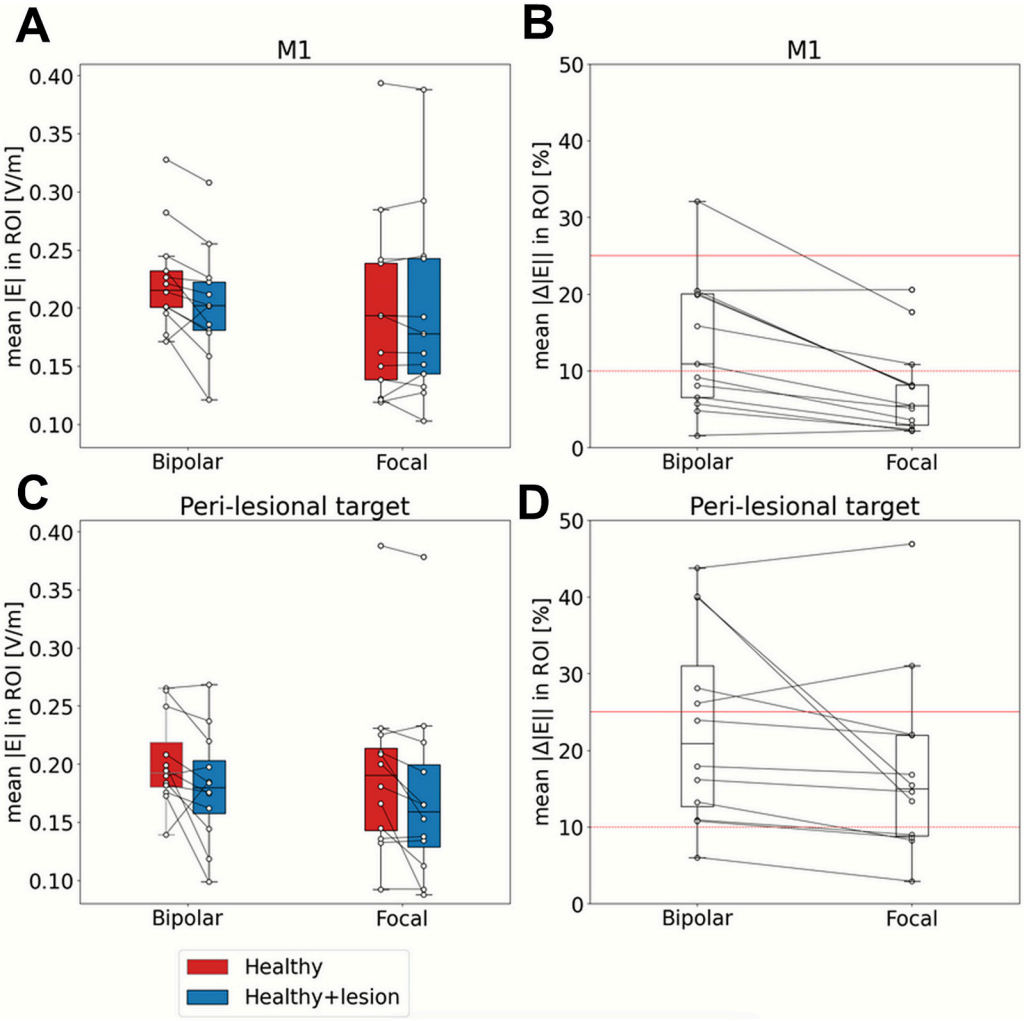

Fig. 3. Change of the electric field strengths (|E|) within the ROIs after adding artificial lesions to the healthy head models. (A and C) Boxplots of the average E-field strengths in the ROIs before (Healthy) and after (Healthy + lesion) adding artificial lesions for montages targeting hand representation of the left primary motor cortex (M1; A) and the *peri*-lesional target (C). (B and D) Boxplots of the averages of the location-wise E-field strength differences in the ROIs in % for montages targeting M1 (B) and the *peri*-lesional target (D).

Table 1
Change of the average E-field in the ROI (eq. (3) after adding artificial lesions to the healthy head models.

	mean [SD]	min–max	t	*P*
M1				
Δ mean |E| [V/m]				
Bipolar	−0.018 [0.021]	−0.056–0.031	−3.07	**0.010**
Focal	0.000 [0.010]	−0.018–0.021	−0.01	1.00
Bipolar vs. Focal	−0.018 [0.017]	−0.041–0.023	−3.71	**0.003**
|Δ mean |E|| [%]				
Bipolar	11 [8.4]	0.1–31	n/a	n/a
Focal	4.7 [5.5]	0.3–17	n/a	n/a
Peri-lesional target				
Δ mean |E| [V/m]				
Bipolar	−0.022 [0.033]	−0.080–0.045	−2.14	0.056
Focal	−0.020 [0.025]	−0.079–0.008	−2.72	**0.020**
Bipolar vs. Focal	−0.001 [0.028]	−0.063–0.044	−0.13	0.90
|Δ mean |E|| [%]				
Bipolar	16 [14]	1.2–43	n/a	n/a
Focal	12 [14]	0.1–47	n/a	n/a

Note: M1, hand representation of the left primary motor cortex; SD, standard deviation

3.2. *Differences in E-fields between homogeneous- and realistic-lesion head models*

The linear fits of conductivity against MD revealed consistent slope and intercept estimates across patients (slope: mean = 0.76 S•s/mm^3, SD = 0.032 S•s/mm^3, 0.68–0.80 S•s/mm^3; intercept: mean = -0.40 S/m, SD = 0.061 S/m, −0.55 – −0.31 S/m; R^2 [including WM and cCSF]: mean = 0.48, SD = 0.05, 0.37–0.55; see Supp. Fig. 8 for linear fits for a representative patient). Inside the lesion masks, the median lesion conductivities estimated via the diffusion-to-conductivity mapping for each patient showed substantial variability within and across patients (mean = 0.99 S/m, SD = 0.26 S/m, 0.48–1.38 S/m; Supp. Fig. 9). The lesion conductivities of the realistic-lesion head models were lower on average by 0.53–1.07 S/m (mean = 0.80 S/m, SD = 0.16 S/m).

Global metrics: We observed only small differences in the global metrics of the E-fields between the homogeneous- and realistic-lesion head models (peak 95 % |E|: max = 10 %, Supp. Fig. 10; 75 % focality |E|: max = 9.1 %; Supp. Fig. 11).

Effects on the average E-field in the ROIs (Δmean |E|; eq. (3): As for montages targeting M1, we found mostly small and some moderate differences in the average E-fields within the ROIs when changing from homogenous- to realistic-lesion modeling (Fig. 5A; Table 4). Modifying the lesion model resulted in a maximum of 12 % and 4.4 % difference in

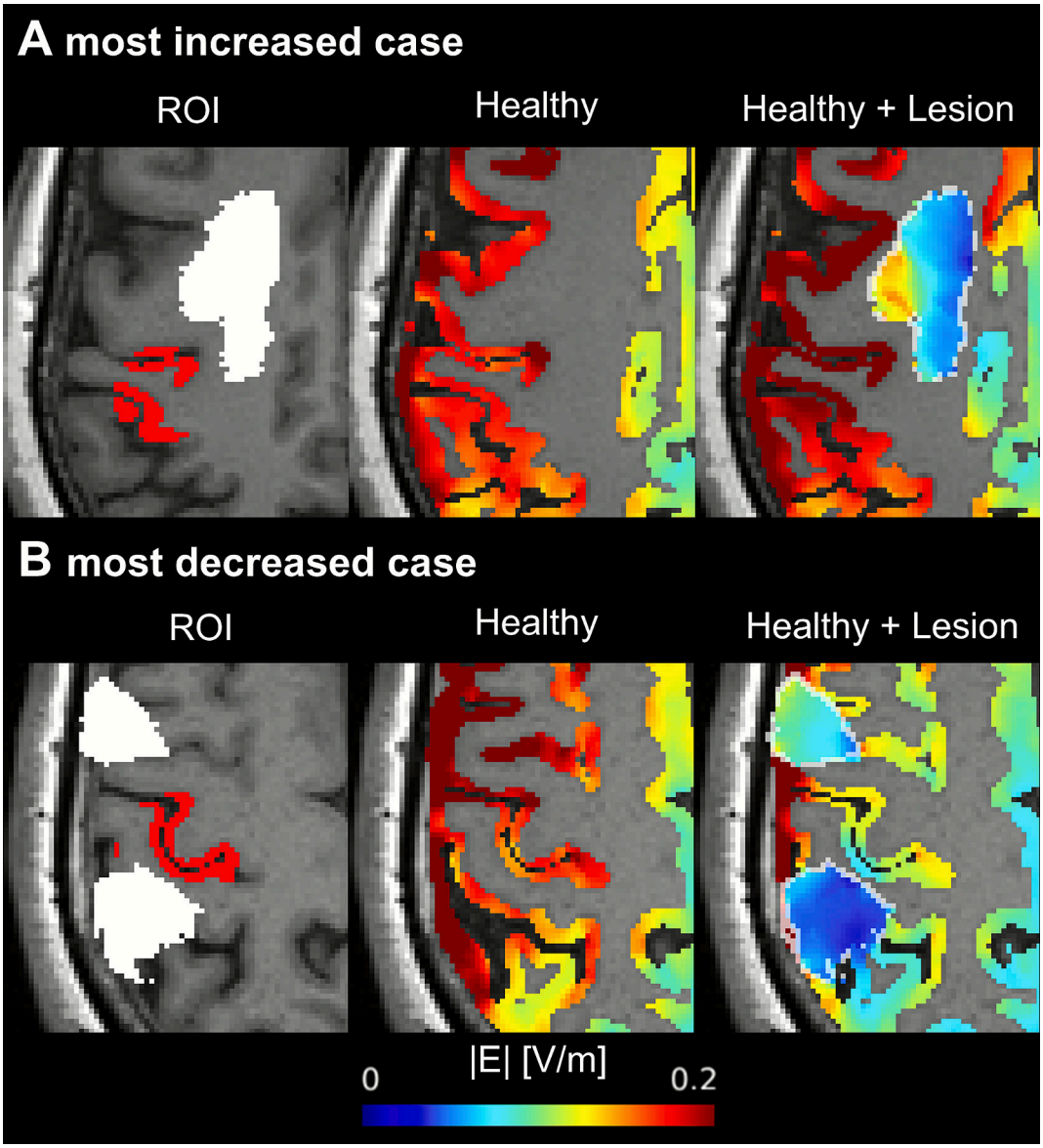

Fig. 4. Simulated electric fields (E-fields) in representative healthy controls with bipolar montage targeting hand representation of the left primary motor cortex. (A) and (B) show the most increased and decreased, respectively, cases in mean E-field strengths within the ROIs after adding artificial lesions. The left panels show the location of ROIs (red area) and lesions (white area). The middle panels show the simulated E-fields in the healthy head models, while the right panels represent those in the healthy head models with artificial lesions. The added lesions are surrounded by white lines. (For interpretation of the references to colour in this figure legend, the reader is referred to the web version of this article.)

average E-field strengths for the bipolar and focal montages, respectively. The average E-field strengths were significantly increased for the bipolar montage, but not for the focal one. That increase was significantly stronger in the bipolar montage compared to the focal one.

In montages targeting the perilesional target, mostly small to moderate differences in the average E-field strengths within the ROIs were observed after converting the lesion models from homogenous to realistic (Fig. 5C; Table 4). The maximum differences were 23 % and 41 % for the bipolar and focal montages, respectively. There was no significantly consistent increase or decrease in the average E-field strengths, either for the bipolar or focal montages (see Fig. 6A and B for the most increased and decreased cases, respectively, for the bipolar montage). The changes were not significantly different between the bipolar and focal montages.

We then explored the associations between the inter-individual variability of the difference in the average E-field strengths within the ROIs and the anatomical lesion features (Supp. Table 2). Here, we additionally investigated the correlation with the mean absolute difference in the conductivity within lesions because this value was highly variable across patients. The absolute difference in mean E-field strength between the two lesion models was significantly negatively correlated with the lesion-to-target distance in most montages. In contrast, it was not significantly correlated to the lesion size or the mean absolute difference in the conductivity within lesions in any montage.

Average of the location-wise E-field differences in the ROIs (mean $|\Delta|\mathbf{E}||$; eq. 4): For montages targeting M1, the average of the location-wise E-field strength differences remained mostly small (Fig. 5B; Table 5). In percent, it reached a maximum of 13 % and 9.0 % for the bipolar and focal montages, respectively. It was significantly higher in the bipolar than the focal montages.

In contrast, the average of the location-wise E-field strength differences reached moderate and even large differences in montages targeting the *peri*-lesional target (Fig. 5D; Table 5). The maximum relative difference was 26 % and 40 % for the bipolar and focal montages,

Table 2
Average of the location-wise E-field differences in the ROI (eq. (4) after adding artificial lesions to the healthy head models.

	mean [SD]	min–max	t	*P*
M1				
mean |Δ| *E*|| [V/m]				
Bipolar	0.026 [0.014]	0.003–0.054	n/a	n/a
Focal	0.011 [0.007]	0.003–0.022	n/a	n/a
Bipolar vs. Focal	0.015 [0.010]	−0.001–0.034	5.42	**< 0.001**
mean |Δ| *E*|| [%]				
Bipolar	13 [8.4]	1.6–32	n/a	n/a
Focal	7.5 [5.6]	2.2–21	n/a	n/a
Peri-lesional target				
mean |Δ| *E*|| [V/m]				
Bipolar	0.038 [0.020]	0.013–0.080	n/a	n/a
Focal	0.028 [0.019]	0.003–0.076	n/a	n/a
Bipolar vs. Focal	0.010 [0.019]	−0.021–0.054	1.72	0.11
mean |Δ| *E*|| [%]				
Bipolar	23 [12]	6.0–44	n/a	n/a
Focal	18 [11]	2.9–47	n/a	n/a

Note: M1, hand representation of the left primary motor cortex; SD, standard deviation

Table 3
Correlation between lesion features and average of the location-wise E-field differences in the ROI (eq. (4) after adding artificial lesions to the healthy head models.

	Lesion size $\rho[P]$	Lesion-to-target distance $\rho[P]$
M1		
Bipolar	0.59 [**0.033**]	−0.80 [**0.001**]
Focal	0.64 [**0.019**]	−0.87 [**< 0.001**]
Peri-lesional target		
Bipolar	0.57 [0.055]	−0.70 [**0.011**]
Focal	0.59 [**0.042**]	−0.48 [0.12]

Note: M1, hand representation of the left primary motor cortex; ρ, Spearman's correlation coefficient.

respectively. It was significantly higher in the bipolar montage than the focal one, as in montages targeting M1.

Table 6 shows the correlations between the average of the location-wise E-field strength differences and the anatomical lesion features. It was significantly positively correlated to the lesion size in the two M1 montages, and was significantly negatively correlated to the lesion-to-target distance in all montages.

4. Discussion

In this study, we evaluated the impact of lesions on tDCS-induced E-fields using realistic sizes and shapes of lesion masks from stroke patients. We also assessed the extent to which modeling spatial heterogeneity of lesion conductivity impacts the simulated E-field. Compared to prior studies (Datta et al., 2011; Evans et al., 2023; Galletta et al., 2015; Krishnamurthy et al., 2025; Richardson et al., 2015; Minjoli et al., 2017), the use of a larger dataset that also included diffusion MRI enabled us to relate interindividual differences in lesion size and composition to the resulting effects on the tDCS-induced E-fields. We found that adding lesions to a healthy head model can affect the E-field near the targeted region by up to 47 % depending on the size of the lesions and the distance of a lesion from the target location. Diffusion-to-conductivity mapping (realistic-lesion head models) revealed high variability in lesion conductivity within and across the stroke patients, and incorporating heterogeneous conductivity introduced additional mostly small to moderate differences in the E-field in the target location compared to homogeneous-lesion head models. These differences were most pronounced for bipolar montages, larger lesional volumes, and closer locations of the lesions relative to the stimulation target. Considering that lesions in patients after stroke are often close to the target area, as in our dataset on stroke-induced aphasia (e.g., Fig. 6B), we recommend acquiring dMRI data prior to tDCS to apply realistic-lesion head models in future stroke studies employing prospective or retrospective modeling of tDCS-induced E-fields.

4.1. Lesions can both increase and decrease the E-field nearby the target region

Adding homogenous lesions to a healthy head model led to both increases and decreases in the E-field within the ROI. This aligns with a previous simulation study that systematically placed artificial lesions around the ROI. That study showed that the E-field was increased when the lesion was aligned with the main E-field direction and decreased when located in its orthogonal direction (Evans et al., 2023). Our results extended this previous finding by showing that such increase or decrease can also occur for realistic lesion shapes and lesion-to-target distances in stroke patients. These findings indicate that the direction of lesion impact on the E-field in the target region cannot be predicted without simulations and underscore the need for using individual head models to individually optimize tDCS parameters in stroke patients.

Minjoli et al., (2017) reported a reduction of the average cortical field strength in two stroke patients compared to a healthy control. While this is in line with the reduction of the 95 % peak E-field that was observed here in most cases when adding an artificial lesion to the healthy controls, we observed that the E-field within the target region can both increase and decrease. We speculate that further anatomical differences between the brains of the healthy control and stroke patients might have additionally contributed to the marked difference seen in Minjoli et al., (2017). In particular, increased atrophy levels in the stroke patients might have promoted current shunting through CSF, further reducing the E-field in gray matter.

Adding homogeneous lesions altered the E-field within the ROIs by an average of 7.5–23 % depending on the electrode montage. This change is large given that a previous simulation study reported an average change of ~ 5 % within ROIs when artificial lesions were added to healthy head models (Evans et al., 2023). This difference is probably due to the difference in the investigated lesion size and the lesion-to-target distance. In Evans et al. (2023), artificial lesions were added with spheres ranging from 4 to 24 mm in radius (268–57,906 mm^3), while the lesional volume in our study was larger (7,181–110,304 mm^3). Furthermore, while that study did not consider the case that lesions overlap with the ROI, we found that this can happen in both M1 and the *peri*-lesional target (lesion-to-target distance < 12.5 mm in Supp. Fig. 5B). Supporting these, the average of the location-wise E-field differences in the ROIs (eq. (4) was correlated to the lesion size and lesion-to-target distance in most montages, showing that these factors modulate the degree by which lesions change the tDCS-induced E-field in the ROIs. In summary, we found that, even with the assumption of homogeneous lesions, these lesions can lead to moderate and in some instances large increases or decreases of the E-field in the target regions, highlighting the need for personalized head models for stroke patients.

4.2. Diffusion-to-conductivity mapping revealed substantial heterogeneity in the conductivity of lesions across the patients

One further important aspect is the heterogeneity of the lesion conductivity within and across the stroke patients. The applied diffusion-to-conductivity mapping indeed revealed high intra- and inter-individual variability in the lesion conductivities. A previous *meta*-analysis on lesion conductivity also showed large variability in the lesion conductivity across five studies (0.10–1.77 S/m; McCann et al., (2019)).

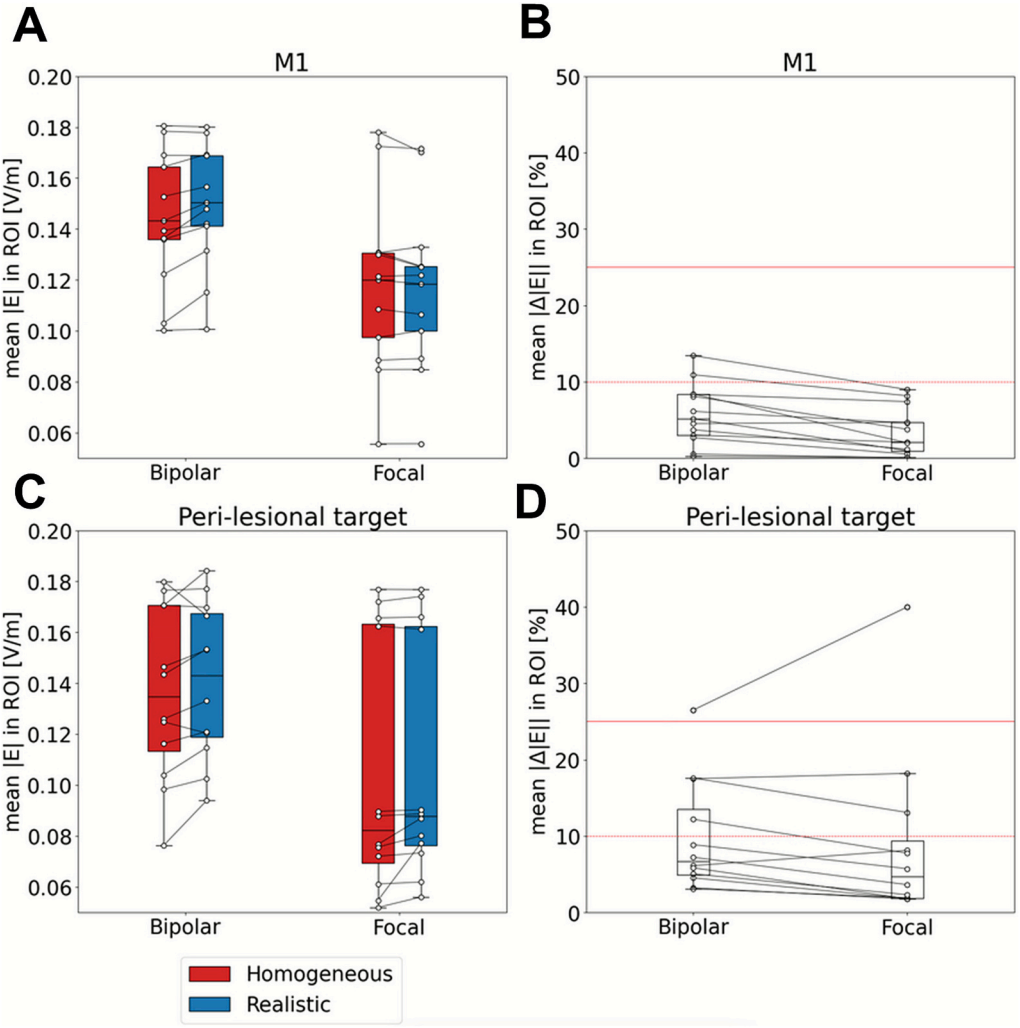

Fig. 5. Change of the electric field strengths (|E|) within the ROIs after changing the lesion conductivity from homogeneous to realistic in stroke patients. (A and C) Boxplots of the average E-field strengths in the ROIs in the homogenous- and realistic-lesion head models for montages targeting hand representation of the left primary motor cortex (M1; A) and the *peri*-lesional target (C). (B and D) Boxplots of the averages of the location-wise E-field strength differences in the ROIs in % for montages targeting M1 (B) and the *peri*-lesional target (D).

Table 4
Change of the average E-field in the ROI (eq. (3) after modifying homogenous- to realistic-lesion head models.

	mean [SD]	min–max	t	*P*
M1				
Δ mean |E| [V/m]				
Bipolar	0.004 [0.004]	−0.001–0.012	3.45	**0.005**
Focal	−0.001 [0.003]	−0.008–0.003	−1.48	0.16
Bipolar vs. Focal	0.006 [0.003]	0.000–0.012	5.74	**< 0.001**
Δ| mean |E|| [%]				
Bipolar	3.5 [3.6]	0.1–12	n/a	n/a
Focal	1.7 [1.5]	0.0–4.4	n/a	n/a
Peri-lesional target				
Δ mean |E| [V/m]				
Bipolar	0.005 [0.008]	−0.013–0.018	1.94	0.079
Focal	0.004 [0.006]	−0.001–0.022	2.00	0.071
Bipolar vs. Focal	0.001 [0.006]	−0.012–0.009	0.51	0.62
Δ| mean |E|| [%]				
Bipolar	6.5 [5.7]	0.3–23	n/a	n/a
Focal	6.3 [11]	0.1–41	n/a	n/a

Note: M1, hand representation of the left primary motor cortex; SD, standard deviation

Table 5
Average of the location-wise E-field differences in the ROI (eq. (4) after modifying homogenous- to realistic-lesion head models.

	mean [SD]	min–max	t	*P*
M1				
mean |Δ| *E*|| [V/m]				
Bipolar	0.007 [0.004]	0.000–0.013	n/a	n/a
Focal	0.003 [0.003]	0.000–0.010	n/a	n/a
Bipolar vs. Focal	0.004 [0.003]	0.000–0.009	5.15	**< 0.001**
mean |Δ| *E*|| [%]				
Bipolar	5.8 [3.8]	0.3–13	n/a	n/a
Focal	3.4 [3.0]	0.1–9.0	n/a	n/a
Peri-lesional target				
mean |Δ| *E*|| [V/m]				
Bipolar	0.010 [0.007]	0.004–0.026	n/a	n/a
Focal	0.006 [0.006]	0.001–0.022	n/a	n/a
Bipolar vs. Focal	0.004 [0.005]	−0.004–0.018	3.09	**0.010**
mean |Δ| *E*|| [%]				
Bipolar	9.8 [7.0]	3.1–26	n/a	n/a
Focal	8.8 [11]	1.8–40	n/a	n/a

Note: M1, hand representation of the left primary motor cortex; SD, standard deviation

Table 6
Correlation between lesion features and average of the location-wise E-field differences in the ROI (eq. (4) after modifying homogenous- to realistic-lesion head models.

	Lesion size $\rho[P]$	Lesion-to-target distance $\rho[P]$	Conductivity difference $\rho[P]$
M1			
Bipolar	0.72	−0.82 [< **0.001**]	−0.35 [0.24]
Focal	[**0.006**]	−0.94 [< **0.001**]	−0.07 [0.82]
	0.60		
Peri-lesional target	[**0.031**]	−0.79 [**0.002**]	0.11 [0.73]
Bipolar		−0.94 [< **0.001**]	0.15 [0.63]
Focal	0.29 [0.35]		
	0.27 [0.40]		

Note: M1, hand representation of the left primary motor cortex; ρ, Spearman's correlation coefficient

Together with our results, these observations suggest that lesion conductivity values should be individualized based on lesion properties to improve the simulation accuracy of E-field in stroke patients. The *meta*-analysis also reported that the weighted mean of the conductivity of lesions across the studies was 0.88 S/m [SD = 0.38 S/m]. This value is comparable to the group-averaged median conductivity within the lesions in our study (0.99 S/m [SD = 0.26 S/m]), supporting the validity of our method.

Modifying from homogenous- to realistic-lesion head models induced only small E-field differences in most stroke patients. Correspondingly, average group-level E-fields changes were only weak. However, at the individual level, up to one third of patients (4 out of 12) showed moderate or large differences in E-field between these two head models. When E-field calculations are aimed at personalized treatment planning, they need to be accurate on the individual level, suggesting a potential benefit of lesion conductivities estimated from diffusion MRI in those cases. In addition, the physiological and behavioral effects of tES may have a non-linear dependence on the strength of the induced E-fields (Caulfield et al., 2022; Mirjalili et al., 2025), which can make moderate differences clinically relevant.

4.3. The degree of E-field differences in the ROIs between homogeneous- and realistic-lesion models was dependent on the lesion size and lesion-to-target distance

The average of the location-wise E-field differences in the ROIs (eq. (4) were positively correlated with lesion size in several montages. This is consistent with a previous simulation study (Evans et al., 2023), and expected because the differences in the lesion conductivities between the two head models are more widespread if the lesions are large. The more widespread differences in conductivity would make the E-field within the ROI more susceptible to the differences in the lesion model. Thus, using realistic lesion modeling can be more important as the lesion size increases.

In addition, these differences were negatively correlated with the lesion-to-target distance across all montages. As in previous (Evans et al., 2023) and our studies, the effect of lesions on the simulated E-field within the ROI is larger if the lesions are closer. Therefore, the E-field within the ROI would be also more affected by the differences in lesion model with shorter lesion-to-target distance. Given that significant correlations were observed in lesion-to-target distance more consistently than in lesion size, the lesion proximity may be more critical determinant of the |E| differences between the homogenous- and realistic-lesion head models than lesion size.

4.4. Modifying the lesion model had a larger impact on |e| more in the bipolar montages than focal montages

The mean absolute change in |E| within the ROI after modifying the lesion model from homogeneous to realistic was consistently larger in the bipolar than focal montages. This likely reflects the fact that bipolar montages distribute tDCS-induced current more broadly within the brain than focal montages. Consequently, lesions located anywhere nearby this more widespread current pathway in bipolar montage would be more likely to influence current flow than focal montages. These findings suggest that montage selection is another key determinant of whether realistic-lesion modeling substantially alters simulated E-fields, and that bipolar montages, in particular, warrant cautious head modeling in stroke populations.

4.5. Limitations

This study has some limitations. First, we used head models of age-matched healthy individuals as controls. Although this approach helps to account for age-related differences in brain morphology, previous studies have shown that cortical atrophy can be more pronounced in stroke patients (Minjoli et al., 2017), and head size or brain volume may still differ even when age is controlled. For this reason, we did not directly compare E-fields between stroke patients and healthy controls. Instead, we compared E-fields within group: head models of healthy controls with and without realistic lesion masks, and those of stroke patients using two different lesion models. Thus, we do not think that morphological differences between stroke patients and healthy controls affect the validity of our conclusions.

We also acknowledge that the sample size (n = 13) in our study was relatively small, even it is comparable to or larger than that of previous modeling studies in stroke patients (n = 2–16; Carla Piastra et al., 2021; Evans et al., 2023; Handiru et al., 2021; Minjoli et al., 2017). This approach may have been insufficient to provide robust results in our correlation analyses, where we opted not to apply multiple comparisons corrections to maintain sensitivity at the cost of an increased risk of Type I errors. Therefore, the findings from these exploratory analyses should be interpreted with caution. Future studies with larger samples will be necessary to confirm the replicability of our findings. It would also be valuable to develop a model predicting the lesion effect on E-fields based on lesion features, including lesion locations (Evans et al., 2023), from larger datasets of stroke patients.

4.6. Future directions

Although the realistic-lesion head model employed in this study is promising for individual simulations of tDCS-induced current in stroke patients, the underlying diffusion-to-conductivity mapping has not yet been validated and may not fully capture the complex microstructural compositions of chronic lesions, including scar tissue formation and gliosis. However, the linear relationship in the model of Tuch et al., (2001) is derived from a general model of transport processes in two-phase anisotropic media and will hold as long as the intracellular space is effectively shielded by highly resistive cell membranes. Therefore, we do not see an obvious cause that would render the latter condition invalid for chronic stroke lesions. Nevertheless, future validation, using e.g., magnetic resonance current density imaging (Gregersen et al., 2024), will still be important to confirm the accuracy of the estimated E-field from the realistic-lesion head model.

Beyond methodological validation, establishing the clinical utility of our approach will be essential. While our findings demonstrated that replacing homogeneous-lesion head models with realistic-lesion head models can change simulated E-fields, it remains to be demonstrated whether such changes can benefit neurorehabilitation in stroke patients. It is also important to note that factors beyond E-field can affect the intra- or inter-individual variability in tDCS effect, including age,

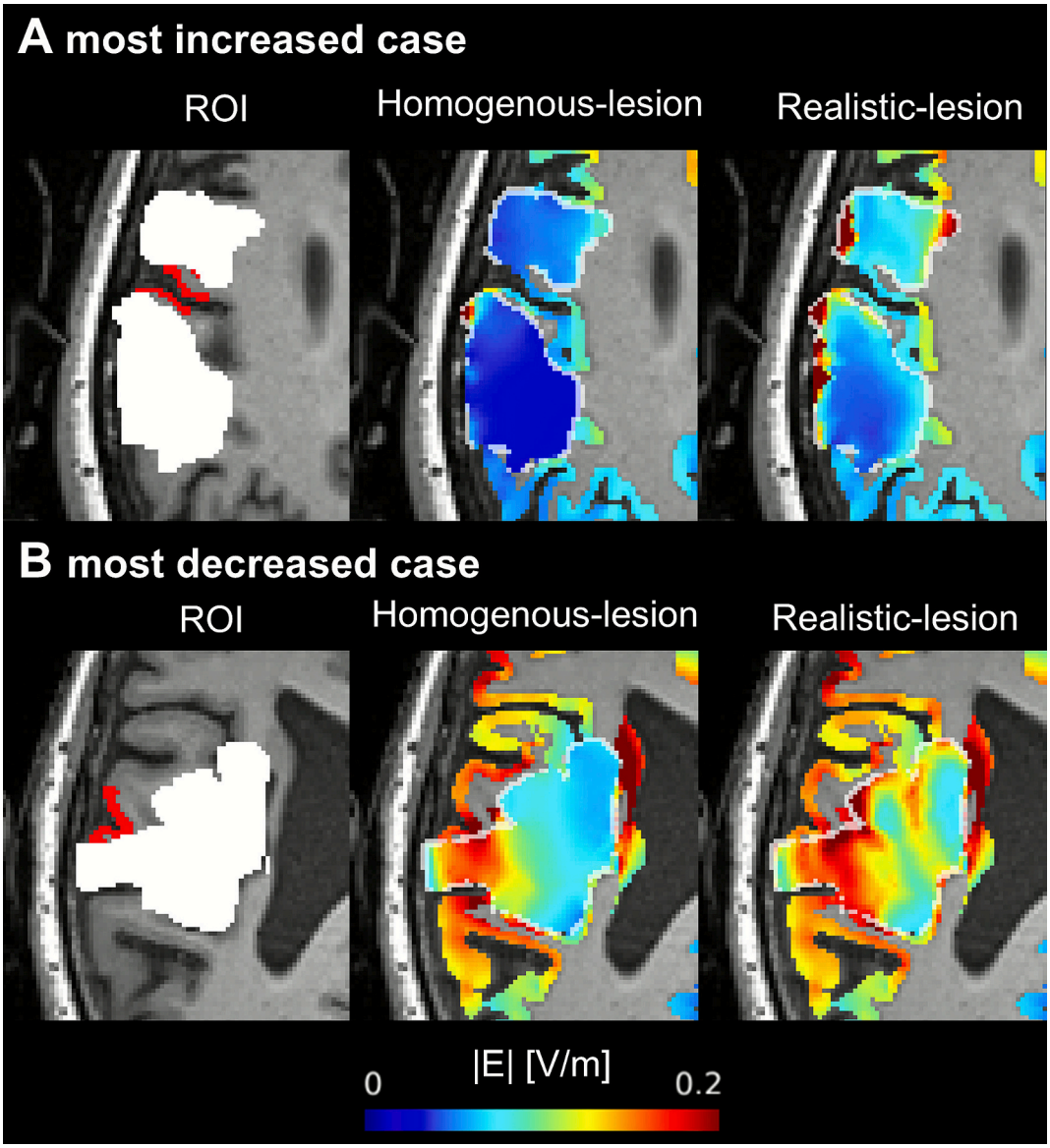

Fig. 6. Simulated electric fields (E-fields) in representative stroke patients with bipolar montage targeting the *peri*-lesional target. (A) and (B) show the cases in which the mean E-field strengths within the ROIs increased and decreased the most, respectively, after changing the lesion models from homogeneous to realistic. The left panels show the location of ROIs (red area) and lesions (white area). The middle panels show the simulated E-fields in the homogeneous-lesion head models, while the right panels represent those in the realistic-lesion head models. The added lesions are surrounded by white lines. (For interpretation of the references to colour in this figure legend, the reader is referred to the web version of this article.)

genetics, brain state, and lesion characteristics (López-Alonso et al., 2014; Guerra et al., 2020; Huang et al., 2017). Future studies should therefore test whether using realistic- instead of homogenous-lesion head models increases the correlation of the E-fields with neurophysiological and behavioral tES effects in larger samples than available here. Such studies would be a critical step towards prospective studies confirming whether the realistic-lesion head models can yield clinically relevant benefits.

4.7. Conclusions

Our study demonstrated that homogenous-lesion head models can alter the E-field nearby the target location by up to 47 % compared to healthy head models. Our diffusion-to-conductivity mapping approach revealed substantial variability in the conductivity of lesions both within and across stroke patients. Modifying the lesion model from homogeneous to realistic produced mostly small to moderate differences, particularly when bipolar montages were applied, lesions were larger, or lesions were located closer to the target region. These findings indicate that realistic-lesion head model should be employed to simulate tDCS-induced E-field when aiming to design individualized stimulation protocols accurately for stroke patients. Incorporating this model may enhance the precision and efficacy of personalized tDCS interventions in stroke rehabilitation, an approach to be validated in future prospective studies.

Declaration of generative AI and AI-assisted technologies in the writing process

During the preparation of this manuscript, the authors used language editing tools (ChatGPT and DeepL) to improve readability and clarity. All content was subsequently reviewed and revised by the authors, who take full responsibility for the final version of the article.

CRediT authorship contribution statement

Ikko Kimura: Writing – original draft, Visualization, Validation, Software, Methodology, Conceptualization. **Marcus Meinzer:** Writing – review & editing, Writing – original draft, Investigation. **Daria Antonenko:** Writing – review & editing, Methodology, Data curation. **Robert Darkow:** Writing – review & editing, Investigation, Data curation. **Agnes Flöel:** Writing – review & editing, Supervision, Project administration, Funding acquisition. **Axel Thielscher:** Writing – review & editing, Supervision, Project administration, Methodology, Funding acquisition, Conceptualization.

Declaration of competing interest

The authors declare that they have no known competing financial interests or personal relationships that could have appeared to influence the work reported in this paper.

Acknowledgments

This work was supported by the German Research Foundation (Research Unit 5429/1 (467143400), AF 379/34-1, AF 379/35-1, MM 3161/5-1, MM 3161/6-1, DA 1103/5-1, AT 1330/6-1, AT 1330/7-1), and Bundesministerium für Bildung und Forschung (AF: FKZ0315673A, 01GY1144; 01GQ1424A, 01GQ1420B; AF and MM: 01EO0801). DA was supported by the Heisenberg Programme of the German Research Foundation (project number: 539593253). AT was supported by the Lundbeck foundation (grant R313-2019-622).

Appendix A. Supplementary data

Supplementary data to this article can be found online at https://doi.org/10.1016/j.nicl.2025.103931.

Data availability

The data that has been used is confidential.

References

Antal, A., Alekseichuk, I., Bikson, M., Brockmöller, J., Brunoni, A.R., Chen, R., Cohen, L. G., Dowthwaite, G., Ellrich, J., Flöel, A., Fregni, F., George, M.S., Hamilton, R., Haueisen, J., Herrmann, C.S., Hummel, F.C., Lefaucheur, J.P., Liebetanz, D., Loo, C. K., McCaig, C.D., Miniussi, C., Miranda, P.C., Moliadze, V., Nitsche, M.A., Nowak, R., Padberg, F., Pascual-Leone, A., Poppendieck, W., Priori, A., Rossi, S., Rossini, P.M., Rothwell, J., Rueger, M.A., Ruffini, G., Schellhorn, K., Siebner, H.R., Ugawa, Y., Wexler, A., Ziemann, U., Hallett, M., Paulus, W., 2017. Low intensity transcranial electric stimulation: Safety, ethical, legal regulatory and application guidelines. Clin. Neurophysiol. off. J. Int. Fed. Clin. Neurophysiol. 128, 1774–1809. https://doi.org/10.1016/j.clinph.2017.06.001.

Antonenko, D., Thielscher, A., Saturnino, G.B., Aydin, S., Ittermann, B., Grittner, U., Flöel, A., 2019. Towards precise brain stimulation: is electric field simulation related to neuromodulation? Brain Stimulat. 12, 1159–1168. https://doi.org/10.1016/j.brs.2019.03.072.

Baker, J.M., Rorden, C., Fridriksson, J., 2010. Using transcranial direct-current stimulation to treat stroke patients with aphasia. Stroke 41, 1229–1236. https://doi.org/10.1161/STROKEAHA.109.576785.

Baumann, S.B., Wozny, D.R., Kelly, S.K., Meno, F.M., 1997. The electrical conductivity of human cerebrospinal fluid at body temperature. I.E.E.E. Trans. Biomed. Eng. 44, 220–223. https://doi.org/10.1109/10.554770.

Brady, M.C., Kelly, H., Godwin, J., Enderby, P., Campbell, P., 2016. Speech and language therapy for aphasia following stroke. Cochrane Database Syst. Rev. 2016, CD000425. https://doi.org/10.1002/14651858.CD000425.pub4.

Brady, M.C., Mills, C., Prag Øra, H., Novaes, N., Becker, F., Constantinidou, F., Flöel, A., Sunnerhagen, K.S., Isaksen, J., Jagoe, C., Jesus, L.M., Marangolo, P., Meinzer, M., van der Meulen, I., Campbell, P., Ho, L., Hussain, S., Hilari, K., 2025. European Stroke Organisation (ESO) guideline on aphasia rehabilitation. Eur. Stroke J. 23969873241311025. https://doi.org/10.1177/23969873241311025.

Branscheidt, M., Hoppe, J., Zwitserlood, P., Liuzzi, G., 2018. tDCS over the motor cortex improves lexical retrieval of action words in poststroke aphasia. J. Neurophysiol. 119, 621–630. https://doi.org/10.1152/jn.00285.2017.

Breitenstein, C., Grewe, T., Flöel, A., Ziegler, W., Springer, L., Martus, P., Huber, W., Willmes, K., Ringelstein, E.B., Haeusler, K.G., Abel, S., Glindemann, R., Domahs, F., Regenbrecht, F., Schlenck, K.-J., Thomas, M., Obrig, H., de Langen, E., Rocker, R., Wigbers, F., Rühmkorf, C., Hempen, I., List, J., Baumgaertner, A., FCET2EC study group, 2017. Intensive speech and language therapy in patients with chronic aphasia after stroke: a randomised, open-label, blinded-endpoint, controlled trial in a health-care setting. Lancet Lond. Engl. 389, 1528–1538. https://doi.org/10.1016/S0140-6736(17)30067-3.

Carla Piastra, M., van der Cruijsen, J., Piai, V., Jeukens, F.E.M., Manoochehri, M., Schouten, A.C., Selles, R.W., Oostendorp, T., 2021. ASH: an Automatic pipeline to generate realistic and individualized chronic Stroke volume conduction Head models. J. Neural Eng. 18. https://doi.org/10.1088/1741-2552/abf00b.

Caulfield, K.A., Indahlastari, A., Nissim, N.R., Lopez, J.W., Fleischmann, H.H., Woods, A. J., George, M.S., 2022. Electric Field Strength from Prefrontal Transcranial Direct Current Stimulation Determines Degree of Working memory Response: a potential Application of Reverse-Calculation Modeling? Neuromodulation 25, 578–587. https://doi.org/10.1111/ner.13342.

Crosson, B., Rodriguez, A.D., Copland, D., Fridriksson, J., Krishnamurthy, L.C., Meinzer, M., Raymer, A.M., Krishnamurthy, V., Leff, A.P., 2019. Neuroplasticity and aphasia treatments: new approaches for an old problem. J. Neurol. Neurosurg. Psychiatry 90, 1147–1155. https://doi.org/10.1136/jnnp-2018-319649.

Darkow, R., Martin, A., Würtz, A., Flöel, A., Meinzer, M., 2017. Transcranial direct current stimulation effects on neural processing in post-stroke aphasia. Hum. Brain Mapp. 38, 1518–1531. https://doi.org/10.1002/hbm.23469.

Datta, A., Baker, J.M., Bikson, M., Fridriksson, J., 2011. Individualized model predicts brain current flow during transcranial direct-current stimulation treatment in responsive stroke patient. Brain Stimulat. 4, 169–174. https://doi.org/10.1016/j.brs.2010.11.001.

Duering, M., Adam, R., Wollenweber, F.A., Bayer-Karpinska, A., Baykara, E., Cubillos-Pinilla, L.Y., Gesierich, B., Araque Caballero, M.Á., Stoecklein, S., Ewers, M., Pasternak, O., Dichgans, M., 2020. Within-lesion heterogeneity of subcortical DWI lesion evolution, and stroke outcome: a voxel-based analysis. J. Cereb. Blood Flow Metab. Off. J. Int. Soc. Cereb. Blood Flow Metab. 40, 1482–1491. https://doi.org/10.1177/0271678X19865916.

El Hachioui, H., Lingsma, H.F., van de Sandt-Koenderman, M.W.M.E., Dippel, D.W.J., Koudstaal, P.J., Visch-Brink, E.G., 2013. Long-term prognosis of aphasia after stroke. J. Neurol. Neurosurg. Psychiatry 84, 310–315. https://doi.org/10.1136/jnnp-2012-302596.

Elsner, B., Kugler, J., Pohl, M., Mehrholz, J., 2019. Transcranial direct current stimulation (tDCS) for improving aphasia in adults with aphasia after stroke. Cochrane Database Syst. Rev. 5, CD009760. https://doi.org/10.1002/14651858.CD009760.pub4.

Evans, C., Johnstone, A., Zich, C., Lee, J.S.A., Ward, N.S., Bestmann, S., 2023. The impact of brain lesions on tDCS-induced electric fields. Sci. Rep. 13, 19430. https://doi.org/10.1038/s41598-023-45905-7.

Flöel, A., Meinzer, M., Kirstein, R., Nijhof, S., Deppe, M., Knecht, S., Breitenstein, C., 2011. Short-term anomia training and electrical brain stimulation. Stroke 42, 2065–2067. https://doi.org/10.1161/STROKEAHA.110.609032.

Flöel, A., Rösser, N., Michka, O., Knecht, S., Breitenstein, C., 2008. Noninvasive brain stimulation improves language learning. J. Cogn. Neurosci. 20, 1415–1422. https://doi.org/10.1162/jocn.2008.20098.

Fridriksson, J., Rorden, C., Elm, J., Sen, S., George, M.S., Bonilha, L., 2018. Transcranial Direct Current Stimulation vs Sham Stimulation to Treat Aphasia after Stroke: a Randomized Clinical Trial. JAMA Neurol. 75, 1470–1476. https://doi.org/10.1001/jamaneurol.2018.2287.

Galletta, E.E., Cancelli, A., Cottone, C., Simonelli, I., Tecchio, F., Bikson, M., Marangolo, P., 2015. Use of Computational Modeling to Inform tDCS Electrode Montages for the Promotion of Language Recovery in Post-stroke Aphasia. Brain Stimulat. 8, 1108–1115. https://doi.org/10.1016/j.brs.2015.06.018.

Gregersen, F., Eroğlu, H.H., Göksu, C., Puonti, O., Zuo, Z., Thielscher, A., Hanson, L.G., 2024. MR imaging of the magnetic fields induced by injected currents can guide improvements of individualized head volume conductor models. Imaging Neurosci. 2, 1–15. https://doi.org/10.1162/imag_a_00176.

Guerra, A., López-Alonso, V., Cheeran, B., Suppa, A., 2020. Variability in non-invasive brain stimulation studies: reasons and results. Neurosci. Lett. 719, 133330. https://doi.org/10.1016/j.neulet.2017.12.058.

Handiru, V.S., Mark, D., Hoxha, A., Allexandre, D., 2021. An Automated Workflow for the Electric Field Modeling of high-definition Transcranial Direct Current Stimulation (HD-tDCS) in Chronic Stroke with Lesions. Annu. Int. Conf. IEEE Eng. Med. Biol. Soc. IEEE Eng. Med. Biol. Soc. Annu. Int. Conf. 2021, 6663–6666. https://doi.org/10.1109/EMBC46164.2021.9629584.

Hesse, S., Werner, C., Schonhardt, E.M., Bardeleben, A., Jenrich, W., Kirker, S.G.B., 2007. Combined transcranial direct current stimulation and robot-assisted arm training in subacute stroke patients: a pilot study. Restor. Neurol. Neurosci. 25, 9–15.

Huang, Y.-Z., Lu, M.-K., Antal, A., Classen, J., Nitsche, M., Ziemann, U., Ridding, M., Hamada, M., Ugawa, Y., Jaberzadeh, S., Suppa, A., Paulus, W., Rothwell, J., 2017. Plasticity induced by non-invasive transcranial brain stimulation: a position paper. Clin. Neurophysiol. off. J. Int. Fed. Clin. Neurophysiol. 128, 2318–2329. https://doi.org/10.1016/j.clinph.2017.09.007.

Hunold, A., Haueisen, J., Nees, F., Moliadze, V., 2023. Review of individualized current flow modeling studies for transcranial electrical stimulation. J. Neurosci. Res. 101, 405–423. https://doi.org/10.1002/jnr.25154.

Jiang, J., Truong, D.Q., Esmaeilpour, Z., Huang, Y., Badran, B.W., Bikson, M., 2020. Enhanced tES and tDCS computational models by meninges emulation. J. Neural Eng. 17, 016027. https://doi.org/10.1088/1741-2552/ab549d.

Krishnamurthy, L.C., Krishnamurthy, V., Rodriguez, A.D., McGregor, K.M., Glassman, C. N., Champion, G.S., Rocha, N., Harnish, S.M., Belagaje, S.R., Kundu, S., Crosson, B. A., 2021. Not all Lesioned Tissue is Equal: Identifying Pericavitational areas in

Chronic Stroke with Tissue Integrity Gradation via T2w T1w Ratio. Front. Neurosci. 15, 665707. https://doi.org/10.3389/fnins.2021.665707.
Krishnamurthy, V., Song, S.E., Krishnamurthy, L.C., Roberts, S.R., Han, J.H., Rodriguez, A.D., Belagaje, S.R., Meinzer, M., Crosson, B.A., 2025. Lesion in the path of current flow to target pericavitational and perilesional brain areas: Acute network-level tDCS findings in chronic aphasia using concurrent tDCS/fMRI. Brain Stimulat. 18, 145–147. https://doi.org/10.1016/j.brs.2025.01.024.
Laakso, I., Mikkonen, M., Koyama, S., Hirata, A., Tanaka, S., 2019. Can electric fields explain inter-individual variability in transcranial direct current stimulation of the motor cortex? Sci. Rep. 9, 626. https://doi.org/10.1038/s41598-018-37226-x.
Liuzzi, G., Freundlieb, N., Ridder, V., Hoppe, J., Heise, K., Zimerman, M., Dobel, C., Enriquez-Geppert, S., Gerloff, C., Zwitserlood, P., Hummel, F.C., 2010. The involvement of the left motor cortex in learning of a novel action word lexicon. Curr. Biol. CB 20, 1745–1751. https://doi.org/10.1016/j.cub.2010.08.034.
López-Alonso, V., Cheeran, B., Río-Rodríguez, D., Fernández-Del-Olmo, M., 2014. Inter-individual variability in response to non-invasive brain stimulation paradigms. Brain Stimulat. 7, 372–380. https://doi.org/10.1016/j.brs.2014.02.004.
Martin, A.K., Meinzer, M., Lindenberg, R., Sieg, M.M., Nachtigall, L., Flöel, A., 2017. Effects of Transcranial Direct Current Stimulation on Neural Networks in Young and older adults. J. Cogn. Neurosci. 29, 1817–1828. https://doi.org/10.1162/jocn_a_01166.
McCann, H., Pisano, G., Beltrachini, L., 2019. Variation in Reported Human Head Tissue Electrical Conductivity Values. Brain Topogr. 32, 825–858. https://doi.org/10.1007/s10548-019-00710-2.
Meinzer, M., Darkow, R., Lindenberg, R., Flöel, A., 2016. Electrical stimulation of the motor cortex enhances treatment outcome in post-stroke aphasia. Brain J. Neurol. 139, 1152–1163. https://doi.org/10.1093/brain/aww002.
Meinzer, M., Jähnigen, S., Copland, D.A., Darkow, R., Grittner, U., Avirame, K., Rodriguez, A.D., Lindenberg, R., Flöel, A., 2014. Transcranial direct current stimulation over multiple days improves learning and maintenance of a novel vocabulary. Cortex. J. Devoted Study Nerv. Syst. Behav. 50, 137–147. https://doi.org/10.1016/j.cortex.2013.07.013.
Meinzer, M., Unger, N., Rysop, A.U., Flöel, A., 2025. Transkranielle Gleichstromstimulation bei Aphasie nach Schlaganfall. In: Sidiropoulos, K. (Ed.), Transkranielle Gleichstromstimulation Bei Aphasien Und Erworbenen Sprechstörungen. Springer, Berlin, Heidelberg, pp. 267–289. https://doi.org/10.1007/978-3-662-70454-7_15.
Minjoli, S., Saturnino, G.B., Blicher, J.U., Stagg, C.J., Siebner, H.R., Antunes, A., Thielscher, A., 2017. The impact of large structural brain changes in chronic stroke patients on the electric field caused by transcranial brain stimulation. NeuroImage Clin. 15, 106–117. https://doi.org/10.1016/j.nicl.2017.04.014.
Mirjalili, M., Brooks, H., Ma, C., Lee, A., Bikson, M., Voineskos, A.N., Blumberger, D.M., Fischer, C.E., Flint, A.J., Herrmann, N., Kumar, S., Lanctôt, K., Mah, L., Mulsant, B. H., Pollock, B.G., Rajji, T.K., 2025. Impact of tDCS-induced Electric Fields on slowing Cognitive Decline in older adults with Mild Cognitive Impairment or Remitted Major Depressive Disorder: an Analysis of the PACt-MD Randomized Clinical Trial. Biol. Psychiatry. https://doi.org/10.1016/j.biopsych.2025.09.020.
Mosayebi-Samani, M., Cunha, T., Eroğlu, H.H., Siebner, H.R., Nitsche, M.A., Thielscher, A., 2025. The effect of brain tissue anisotropy on the electric field caused by transcranial electric stimulation: Sensitivity analysis and magnetic resonance electrical impedance tomography. Imaging Neurosci. 3, imag_a_00481. https://doi.org/10.1162/imag_a_00481.
Niemann, F., Riemann, S., Hubert, A.-K., Antonenko, D., Thielscher, A., Martin, A.K., Unger, N., Flöel, A., Meinzer, M., 2024. Electrode positioning errors reduce current dose for focal tDCS set-ups: evidence from individualized electric field mapping. Clin. Neurophysiol. 162, 201–209. https://doi.org/10.1016/j.clinph.2024.03.031.
Palmer, R., Dimairo, M., Cooper, C., Enderby, P., Brady, M., Bowen, A., Latimer, N., Julious, S., Cross, E., Alshreef, A., Harrison, M., Bradley, E., Witts, H., Chater, T., 2019. Self-managed, computerised speech and language therapy for patients with chronic aphasia post-stroke compared with usual care or attention control (big CACTUS): a multicentre, single-blinded, randomised controlled trial. Lancet Neurol. 18, 821–833. https://doi.org/10.1016/S1474-4422(19)30192-9.
Pedersen, P.M., Vinter, K., Olsen, T.S., 2004. Aphasia after stroke: type, severity and prognosis. the Copenhagen aphasia study. Cerebrovasc. Dis. Basel Switz. 17, 35–43. https://doi.org/10.1159/000073896.
Perceval, G., Martin, A.K., Copland, D.A., Laine, M., Meinzer, M., 2020. Multisession transcranial direct current stimulation facilitates verbal learning and memory consolidation in young and older adults. Brain Lang. 205, 104788. https://doi.org/10.1016/j.bandl.2020.104788.
Perceval, G., Martin, A.K., Copland, D.A., Laine, M., Meinzer, M., 2017. High-definition tDCS of the temporo-parietal cortex enhances access to newly learned words. Sci. Rep. 7, 17023. https://doi.org/10.1038/s41598-017-17279-0.
Puonti, O., Van Leemput, K., Saturnino, G.B., Siebner, H.R., Madsen, K.H., Thielscher, A., 2020. Accurate and robust whole-head segmentation from magnetic resonance images for individualized head modeling. Neuroimage 219, 117044. https://doi.org/10.1016/j.neuroimage.2020.117044.
Raymer, A.M., Johnson, R.K., 2024. Effectiveness of Transcranial Direct Current Stimulation as an Adjuvant to Aphasia Treatment following Stroke: evidence from Systematic Reviews and Meta-analyses. Am. J. Speech Lang. Pathol. 33, 3431–3443. https://doi.org/10.1044/2024_AJSLP-23-00312.
Richardson, J., Datta, A., Dmochowski, J., Parra, L.C., Fridriksson, J., 2015. Feasibility of using high-definition transcranial direct current stimulation (HD-tDCS) to enhance treatment outcomes in persons with aphasia. NeuroRehabilitation 36, 115–126. https://doi.org/10.3233/NRE-141199.
Rose, M.L., Nickels, L., Copland, D., Togher, L., Godecke, E., Meinzer, M., Rai, T., Cadilhac, D.A., Kim, J., Hurley, M., Foster, A., Carragher, M., Wilcox, C., Pierce, J.E., Steel, G., 2022. Results of the COMPARE trial of Constraint-induced or Multimodality Aphasia Therapy compared with usual care in chronic post-stroke aphasia. J. Neurol. Neurosurg. Psychiatry 93, 573–581. https://doi.org/10.1136/jnnp-2021-328422.
Stagg, C.J., Nitsche, M.A., 2011. Physiological basis of transcranial direct current stimulation. Neurosci. Rev. J. Bringing Neurobiol. Neurol. Psychiatry 17, 37–53. https://doi.org/10.1177/1073858410386614.
Thielscher, A., Antunes, A., Saturnino, G.B., 2015. Field modeling for transcranial magnetic stimulation: a useful tool to understand the physiological effects of TMS?. In: Annual International Conference of the IEEE Engineering in Medicine and Biology Society (EMBC). Presented at the 2015 37th Annual International Conference of the IEEE Engineering in Medicine and Biology Society (EMBC), pp. 222–225. https://doi.org/10.1109/EMBC.2015.7318340.
Tuch, D.S., Wedeen, V.J., Dale, A.M., George, J.S., Belliveau, J.W., 2001. Conductivity tensor mapping of the human brain using diffusion tensor MRI. Proc. Natl. Acad. Sci. 98, 11697–11701. https://doi.org/10.1073/pnas.171473898.